



Review

Elemental imaging using laser-induced breakdown spectroscopy: A new and promising approach for biological and medical applications

Benoit Busser^{a,b,c,*}, Samuel Moncayo^b, Jean-Luc Coll^a, Lucie Sancey^{a,1}, Vincent Motto-Ros^{b,1}^a Institute for Advanced Biosciences, UGA INSERM U1209 CNRS UMR5309, Grenoble, France^b Institut Lumière Matière, UMR5306, Université Claude Bernard Lyon 1, CNRS, Villeurbanne, France^c Grenoble Alpes University Hospital, Grenoble, France

ARTICLE INFO

Article history:

Received 15 September 2017

Received in revised form 13 November 2017

Accepted 9 December 2017

Keywords:

Elemental imaging

Laser-induced breakdown spectroscopy (LIBS)

Biological tissues

Medical diagnostics

Metal nanoparticles

ABSTRACT

Biological tissues contain various metal and metalloid ions that play different roles in the structure and function of proteins and are therefore indispensable to several vital biochemical processes. In this review, we discuss the broad capability of laser-induced breakdown spectroscopy (LIBS) for *in situ* elemental profiling and mapping of metals in biological materials such as plant, animal and human specimens. These biological samples contain or accumulate metal species and metal-containing compounds that can be detected, quantified, and imaged. LIBS enables performing microanalysis, mapping and depth profiling of endogenous and exogenous elements contained in the tissues with a parts-per-million scale sensitivity and microscopic resolution. In addition, this technology generally requires minimal sample preparation. Moreover, its tabletop instrumentation is compatible with optical microscopy and most elements from the periodic table. Specifically, low- and high-atomic-number elements can be detected simultaneously. Recent advances in space-resolved LIBS are reviewed with various examples from vegetable, animal and human specimens. Overall, the performance offered by this new technology along with its ease of operation suggest innumerable applications in biology, such as for the preclinical evaluation of metal-based nanoparticles and in medicine, where it could broaden the horizons of medical diagnostics for all pathologies involving metals.

© 2017 Elsevier B.V. All rights reserved.

Contents

1. Introduction	71
2. Metals in bio-medicine and conventional imaging strategies	71
3. Principles of space-resolved LIBS	73
4. LIBS imaging of biological tissues	74
4.1. LIBS analysis of plants	74
4.2. Preclinical applications	75
4.3. Medical applications	77
5. Conclusions and perspectives	77
Conflicts of interests	78
Funding	78
References	78

* Corresponding author at: Institute for Advanced Biosciences, UGA/INSERM U 1209/CNRS UMR 5309 Joint Research Center, Site Santé – Allée des Alpes, 38700 Grenoble, France.

E-mail address: bbusser@chu-grenoble.fr (B. Busser).

¹ Co-last authors.

1. Introduction

Over the last two decades, laser-induced breakdown spectroscopy (LIBS) has become a recognized and valuable analytical spectroscopic technique for analyzing the elemental nature of any type of sample, such as a solid, liquid or gas [1,2]. Many additional advantages of LIBS are acknowledged, such as its simplicity and ability to work at room temperature and under ambient pressure conditions; its ability to detect almost every element on the periodic table, including low- and high-Z elements [3]; its high sensitivity reaching the parts-per-million scale for most of the elements; its high dynamic range of detection (from major to trace amounts); and its standoff capabilities [4]. The accessible resolution is ultimately limited by the diffraction limit, which enables reaching the micrometer scale. In addition, since vacuum conditions are not required, there are no sample size or shape restrictions.

LIBS reveals the elemental composition of materials from a single-shot microanalysis (reviewed in [5]) to 2-D characterization (spatial mapping). This technology also has a 3-D capability (including depth profiling) [3]. These common characteristics, together with its table-top instrumentation and fast operation, render LIBS imaging a promising technology for elemental investigations in the fields of biology and medicine. At first, LIBS analysis was mainly developed to analyze the elemental composition of hard materials, with clear industrial and geological applications [4,6–8]. The capability of space-resolved LIBS for studying biological materials was first demonstrated on mineralized or calcified specimens such as gallstones [9], bones and teeth [10,11]. The possibility of imaging soft tissues via LIBS was demonstrated very recently. This development was limited by both the softness and the highly heterogeneous nature of biological tissues as well as the difficulty of mastering laser ablation on such materials.

The capability of LIBS (not space resolved) for biomedical applications was first demonstrated after a matrix transformation (*i.e.*, tissue mixing, drying, and pelleting), which was employed to improve the laser-ablation efficiency and therefore the LIBS signal-to-noise ratio [2]. Different LIBS instruments equipped with nanosecond or femtosecond lasers may be employed, for single or double pulse analysis [12]. In the related literature, LIBS was used to discriminate between normal and malignant canine hemangiosarcoma tumor cells [13] and to diagnose breast cancer [14], colorectal cancer [15], and melanoma [16]. In the last study, the authors measured the elements both in homogenized pellets and tissues obtained from excised skin samples of melanoma-implanted animals. Their results indicated that Mg and Ca were appropriate biomarkers for discriminating melanoma from normal skin, suggesting a potential direct clinical application of LIBS for human tumor diagnosis [16]. Recently, an innovative approach based on an elemental encoded particle assay coupled with femtosecond-LIBS was developed to improve cancer blood biomarker detectability [17]. In plant biology, LIBS was successfully used to discriminate healthy tobacco leaves from Tobacco Mosaic Virus-infected ones [18]. Finally, LIBS was tested to identify different tissues in real time during laser-based surgery. Using *ex vivo* porcine tissues, the authors successfully identified and classified different target tissues (*i.e.*, fat, nerve, muscle and skin) with high sensitivity and specificity [19,20]. Similarly, in hepatic copper (Cu)-accumulation-related disease, *i.e.*, Wilson's disease, LIBS correctly identified diseased tissues based on the Cu/C content ratio, which discriminated pathological liver biopsies from normal tissue [21].

The aim of this review is to present recent advances in space-resolved LIBS, especially imaging, for biological soft materials. After a short description of the importance of metals in biomedicine, a brief review of standard imaging technologies will be presented

before focusing on the capabilities of the LIBS technology for plant, animal and finally human specimens.

2. Metals in bio-medicine and conventional imaging strategies

In biology, metals are essential actors in most of the functions of DNA, RNA and proteins and even help control epigenetic modifications [22]. In other words, metals govern most indispensable life processes. The redox-inactive alkali and alkali earth metals, notably sodium (Na), potassium (K), magnesium (Mg) and calcium (Ca), are dynamic entities that convey signals through fast and orchestrated movements and exchange of metal ion pools. Redox-active transition metals such as zinc (Zn), copper (Cu) and iron (Fe) are known cofactors involved in the maintenance of structural or catalytic roles. Some of them, when dysregulated, can trigger oxidative stress and damage [22,23]. Consequently, metals have multiple biological functions, ranging from catalytic, regulatory, structural, or signaling roles.

Metal homeostasis must be maintained by coordinated uptake, trafficking and efflux pathways that place the required amount of the correct metal at the appropriate place and time in the cell [24]. Analyzing chemical elements, especially metals, *in situ* in normal or diseased tissues is of considerable interest to determine whether they exist at their expected normal concentrations. In general, metal deficiency and excess strongly affect tissues and may lead to severe, if not deadly, diseases.

Some metals are known to be toxic and harmful to living organisms, whether plant or animal. Twenty-six elements from the periodic table were recently reported to be essential for most forms of life (Fig. 1). However, more than 20 additional non-essential chemical elements are naturally detected in humans. Importantly, the nature and concentrations of non-essential elements are highly variable among individuals, mainly depending on the tissue of interest and lifetime personal exposure [25].

Due to the fundamental importance of metals in biology, their *in situ* visualization plays a major part in describing and understanding their biological role in depth. The spatial distribution of specific metals and metal-based compounds is as important as their chemical properties, because both their concentration and localization change in biological systems, and their transport and compartmentalization is critical for effective utilization. The determination of elemental distributions (imaging or mapping) in biological sample surfaces has been of interest for a long time, and new technologies are now enabling such detection in the biological sciences [26,27].

Most of the current imaging techniques rely on (i) methods that employ metal-selective probes/chemical sensors; (ii) mass spectrometric detection; or (iii) “beam” methods that employ light/lasers, electrons, X-rays or energetic particles to measure characteristic radiation [28].

Several metal-selective probes or chemical sensors can be used for imaging metal ions such as Cu^{2+} [29,30], Fe^{3+} [30], Zn^{2+} [31], Cs^+ [32], Al^{3+} [33] or heavy metal ions such as Ag^+ or Hg^{2+} [34]. Mass spectrometric imaging of metals flourished following the integration of solid sampling techniques with element-specific detection techniques such as inductively coupled plasma-mass spectrometry (ICP-MS). Although laser ablation (LA)-ICP-MS has currently reached a technological barrier preventing practical sub-micron imaging, other MS-based methods, such as nano-secondary ion mass spectrometry (SIMS), are gradually providing the means to image metals at the subcellular level [35].

Multiple abnormalities occur in the homeostasis of essential endogenous brain bio-metals (namely, the late first-row transition metals Fe, Cu and Zn) in age-related neurodegenerative disorders such as Parkinson's disease, Alzheimer's disease, Huntington's

1 H hydrogen 200																	2 He helium n.c.						
3 Li lithium 0.1	4 Be beryllium 0.1																	5 B boron 1	6 C carbon 500	7 N nitrogen 10 000	8 O oxygen 10 000	9 F fluorine 100 000	10 Ne neon n.c.
11 Na sodium 0.7	12 Mg magnesium 0.3																	13 Al aluminum 2	14 Si silicon 10	15 P phosphorous 70	16 S sulphur 100	17 Cl chlorine 20 000	18 Ar argon n.c.
19 K potassium 4	20 Ca calcium 0.5	21 Sc scandium 2	22 Ti titanium 5	23 V vanadium 5	24 Cr chromium 4	25 Mn manganese 4	26 Fe iron 20	27 Co cobalt 5	28 Ni nickel 12	29 Cu copper 2	30 Zn zinc 5	31 Ga gallium 3	32 Ge germanium 7	33 As arsenic 8	34 Se selenium 100	35 Br bromine n.c.	36 Kr krypton n.c.						
37 Rb rubidium 10	38 Sr strontium 0.8	39 Y yttrium 4	40 Zr zirconium 12	41 Nb niobium 20	42 Mo molybdenum 8	43 Tc technetium n.c.	44 Ru ruthenium 12	45 Rh rhodium 10	46 Pd palladium 5	47 Ag silver 2	48 Cd cadmium 5	49 In indium 6	50 Sn tin 20	51 Sb antimony 5	52 Te tellurium 30	53 I iodine n.c.	54 Xe xenon n.c.						
55 Cs caesium 1 000	56 Ba barium 3	R.E.E.		72 Hf hafnium 3	73 Ta tantalum 10	74 W tungsten 90	75 Re rhenium 20	76 Os osmium 21	77 Ir iridium 14	78 Pt platinum 70	79 Au gold 12	80 Hg mercury 150	81 Tl thallium 5	82 Pb lead 8	83 Bi bismuth 4	84 Po polonium n.c.	85 At astatine n.c.	86 Rn radon n.c.					
87 Fr francium n.c.	88 Ra radium n.c.	R.E.E.																					

Metals
 Metalloids
 Nonmetals

Fig. 1. Periodic table of the elements and LIBS analysis. Almost all elements, including metals, are detectable within biological tissues via LIBS. The essential chemical elements for most living organisms are displayed as follows: bulk biological elements are in red and essential trace inorganic elements for plants or animals are in purple, according to [25]. Endogenous and exogenous elements already detected in tissues via LIBS in previous biological studies are marked with a black dot. The theoretical LOD is given in parts per million and is indicated by the number in italics under the chemical name of the element. R.E.E.: rare earth elements.

disease and amyotrophic lateral sclerosis. Moreover, these pathologies may be linked to the toxicological effects of heavy metals (e.g., Cd, Pb, Hg), biologically important metals of lower abundance (e.g., Mn), or non-biological metals (e.g., Al) [36]. Accordingly, there is strong interest in the bio-imaging of metals for such neurodegenerative diseases to further understand the disease mechanisms and possibly to identify potential targets for treatments. In this field, Prof. J. S. Becker's group performed pioneering work and published a variety of multi-elemental imaging procedures for studying frozen brain tissues with LA-ICP-MS [37]. Among other major findings, Prof. J. S. Becker and colleagues contributed to unraveling the role of metals in neurodegenerative pathologies, developing advanced methodologies for LA-ICP-MS bio-imaging of metals and quantitative metallomic investigations on brain sections [38–40]. LA-ICP-MS was also employed to analyze the distribution of multiple metals in placental tissue from a low-birth-weight pregnancy, which helped to identify the components of metal mixtures that are colocalized with biological response markers [41]. LA-ICP-MS was used on paraffin-embedded breast tumors to show that the levels of Ca, Cu, Fe and Zn were higher in the tumor areas [42]. To overcome the intrinsic tissue inhomogeneity, the authors deposited a thin coating of metallic Au. Comparing elemental images and histology is of major importance; thus, a method that allows spatially mapping metals in tissue sections using a combination of mass spectrometry and histology was published [43].

X-ray-based imaging technologies are also major tools for the multi-elemental imaging of tissues. Notably, these approaches include particle-induced X-ray emission (PIXE), X-ray fluorescence microscopy (XFM), and energy dispersive X-ray spectroscopy (EDX) [27,35,44]. While microprobe X-ray imaging methods based on electron and proton beams have low sensitivity, synchrotron X-ray fluorescence imaging (SXRF or microXRF) provides very high sensitivity and resolution. Mainly used for Cu, Fe, and Zn imaging, SXRF imaging provides information at the sub-cellular scale reaching resolutions of 10 nm or less. In the neurological field, SXRF enabled discriminating metals distributed along dendrites from

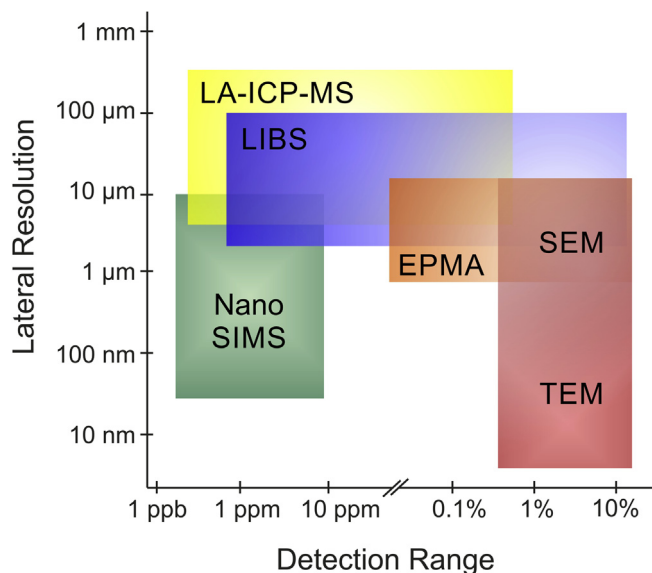


Fig. 2. Diagram of the respective resolutions and levels of detection for the main elemental imaging technologies (space-resolved). LIBS achieves resolution on the micrometer scale with sensitivities in the parts-per-million range. Adapted from [75] with permission. EPMA: electron probe micro-analysis, SEM: scanning electron microscope, TEM: transmission electron microscope.

those localized within the spine [45]. SXRF and LA-ICP-MS techniques both achieve strong sensitivities. Nevertheless, quantification with SXRF remains challenging, and appropriate standards of calibration should be obtained in an adequate matrix [24,46]. Recently, James et al. developed a new technology, named ϕ -XANES, wherein XFM was coupled with X-ray absorption near edge structure (XANES). They applied this technique to study metal coordination at the microscale level in the model organism *Caenorhabditis elegans* [47]. Without any sample preparation, they demonstrated the distribution of Fe redox status in nematodes, with a resolution of 7 μ m [47].

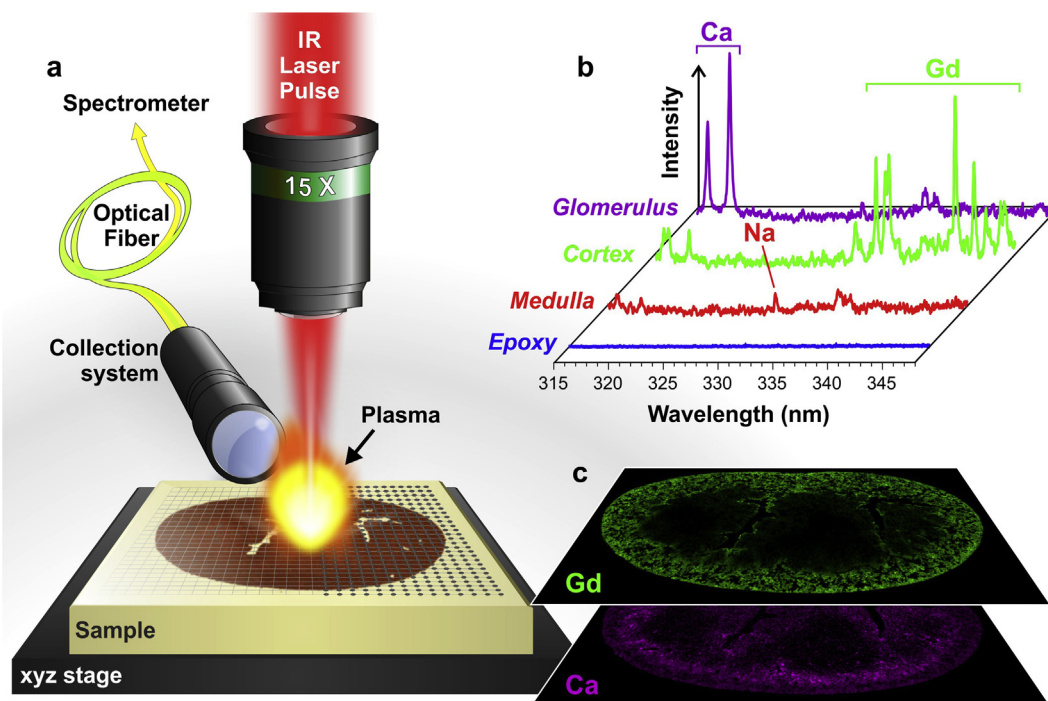


Fig. 3. (a) Schematic view of the LIBS instrument showing the major components: the microscope objective used to focus the laser pulse, the motorized platform supporting the sample and the optical detection system connected to the spectrometer via an optical fiber. (b) Example of single-shot emission spectra covering the 315–345 nm spectral range recorded in different regions of a mouse kidney with the characteristic emission lines of calcium (Ca), sodium (Na), and gadolinium (Gd). (c) Example of relative-abundance images of Gd (green) and Ca (violet) represented with a false color scale. Reproduced with permission from [54].

The identification of elements classified as risk factors or possible causes of neurodegenerative diseases is an important active area of investigation. Two different studies used transmission electron microscope (TEM)-EDX to detect Al in amyloid fibers in the cores of senile plaques located in the hippocampus and temporal lobe [48,49].

Among all these various techniques for elemental imaging, each one has its own advantages and limitations, such as different spatial resolutions and detection limits (Fig. 2), speed of analysis, ease of data processing, level of automatization, accessibility and overall cost of the experiment (instrument/infrastructure). The variety of strategies for metal imaging comes along with a plethora of applications for toxicology, pharmacokinetic monitoring of metal nanoparticles (NPs), neurodegenerative diseases, cancer diagnosis and progression, and medicine in general [27].

The following paragraphs will be focused on recent developments in LIBS imaging for biological tissues, demonstrating that LIBS elemental imaging can be a useful tool for investigating similar scientific challenges.

3. Principles of space-resolved LIBS

LIBS is an analytical method based on the atomic emission spectroscopy (AES) that was first described in the 1960s, shortly after the advent of the laser [50]. High-power laser pulses are focused onto the sample surface, therefore ablating small amounts of the sample (from micrograms to a fraction of a nanogram, depending on the experimental configuration) and creating a plasma. In LIBS, the ablation, atomization and excitation steps occur simultaneously during a single laser pulse. The atoms and ions excited by the high plasma temperature return to lower energy levels by emitting radiation. The emitted light radiation represents a specific elemental response that can be collected by external optical systems and further analyzed with one or more spectrometers

equipped with detectors, generally intensified charge-coupled device (ICCD) cameras (see Fig. 3). The recorded spectrum constitutes a signature that is unique to the sample. Each element has various corresponding emission lines, and their intensities are directly related to the amount of the corresponding element in the sample. In the space-resolved configuration, laser-induced plasmas are continuously generated while scanning the sample surface over the region of interest. Then, elemental profiles, maps or images are obtained after extracting the intensity of the species of interest (i.e., atoms, ions or molecules) from each recorded spectrum (Fig. 3). LIBS-based imaging instrumentation recently experienced several technological breakthroughs. For a complete overview of these advances, see [14,51].

The ability of LIBS to obtain elemental signals from a single laser pulse and a very small amount of material (fraction of a nanogram) confers many advantages to this technology. We can cite its multi-elemental capability, ease of use, and operation under atmospheric pressure. In addition, this is the only all-optical technique that is fully compatible with optical microscopy, providing space-resolved elemental information with a parts-per-million-range sensitivity (accessible for most metals) and a micrometer-scale resolution [52]. Another asset of the technique lies in its acquisition speed. In LIBS, the acquisition rate can be very fast since it is limited only by the detector speed and the laser frequency rate. An acquisition rate of up to kilohertz has already been demonstrated [53]. If required, the relative abundance maps (or profiles) can be calibrated quantitatively using external references [52,54]. This quantification strategy is rather simple as long as the references and the sample to be analyzed are composed of the same matrices. These aspects make LIBS-based imaging highly promising for application in a wide range of fields such as geology, industry and biomedicine, which is the purpose of this review.

Due to the wide variety of elemental responses (emission spectra), which are unique for each element, the detection limits in LIBS can be very different from one element to another. The LODs that

Table 1
Examples of space resolved LIBS studies for soft biological specimens.

Organism	Elements	Pre-treatment	Single Pulse LIBS	References
<i>Plant</i>				
Bermuda grass	Mg, Ca, C, Al, Zn, N, Sr, and Si	None	Nanosecond (10 Hz)	[55]
Vegetables (potato, celery, carrot and eggplant)	27 elements (including Li, Na, Mg, Al, K, Ca, Ti, Cr, Mn, Fe, Cu, Sr, Ba)	None	Nanosecond (10 Hz)	[56]
Sunflower	Ag, Cu	None	Nanosecond (10 Hz)	[57]
	Pb, Mg and Cu	None	Nanosecond	[58]
	Pb, K and Mn	None	Nanosecond	[59]
	Ca	None	Nanosecond (20 Hz) Femtosecond (1 kHz)	[60]
Maize Cornus	Fe	None (dried) None (fresh)	Femtosecond (10 Hz)	[61]
Maize	K, Mg, Na, Ca, P, Si	None	N.A.	[62]
Citrus and Rhododendron	Ca, Fe, Na, K and Mo	None/or heavy-metal particle (colloidal solution) deposition	Nanosecond (100 Hz)	[63]
Apple Pear	P, Cl	None (dried)	20 Hz	[64]
Corn	Ca	None (dried)	Nanosecond	[65]
<i>Animal</i>				
Mouse (kidney)	Na, Ca, Cu, and Gd	None (frozen)	Nanosecond (10 Hz)	[69]
	Gd, Si, Ca and Fe	None (frozen)	Nanosecond (10 Hz)	[70]
	Fe, Na, Gd, Si, P, Mg, Cu, and Ca	Epoxy resin embedding	Nanosecond (10 Hz)	[52]
	Na, Gd	Epoxy resin embedding	Nanosecond (10 Hz)	[71]
	Ca, Na	Epoxy resin embedding	Nanosecond (10 Hz)	[72]
	Gd, Na, Ca	Epoxy resin embedding	Nanosecond (10 Hz)	[54]
Mouse (tumor)	Fe, Mg, Si, Gd	Paraffin embedding	Nanosecond (10 Hz)	[73]
	Au, P	Paraffin embedding	Nanosecond (10 Hz)	[74]
<i>Human</i>				
Healthy Skin Skin tumors	P, Al, Mg, Na, Zn, Si, Fe, and Cu	Paraffin embedding	Nanosecond (10 Hz)	[76]
Tumor (lung)	C, H, O, Na, K	None (frozen)	Nanosecond (10 Hz)	[75]
Skin biopsy Lymph node	Na, P, Al, Ti, Cu, Cr and W	Paraffin embedding	Nanosecond (10 Hz)	[77]

are generally accessible in micro-LIBS and the single-shot configuration are reported in Fig. 1 (expressed in parts per million). These values were estimated by considering the strongest emission lines of each element in the range covering 180–800 nm (generally easy to access with standard spectroscopic devices). While the LODs of nonmetals elements are generally high (≥ 50 –100 ppm), metals and metalloids may be detected at the parts-per-million level, even reaching sub-parts per million for specific elements (e.g., Li, Ca, Mg or Sr). Considering the ablated mass (~ 0.1 ng in micro-LIBS configuration), absolute LODs in the range of hundreds of attograms are accessible for most metals.

4. LIBS imaging of biological tissues

4.1. LIBS analysis of plants

LIBS was used for the *in situ* analysis of major to trace elements that are present in different parts of Bermuda grass (*Cynodon*

dactylon) [55]. The authors demonstrated that *in situ* space-resolved detection/analysis of the elements was possible in plants without any sample preparation. The constitutive elements from different parts (leaf blade, leaf sheath and stem) of a fresh *C. dactylon* plant were analyzed, including Mg, Ca, C, Al, Zn, N, Sr, and Si (Table 1). The concentration of Si was higher in leaf blades than in leaf sheaths and stems. In addition, the LIBS results correlated with the density of phytoliths deposited in different regions of the plant [55].

LIBS analysis was used on fresh vegetables such as potatoes, celery, carrots and eggplants [56]. The authors detected trace and ultra-trace elements and performed a qualitative analysis. The use of UV nanosecond laser for ablation provided sensitive detection. A large number (27) of trace elements were identified (Table 1), including organic elements (H, C, N, O) and inorganic elements, including metals (Li, Na, Mg, Al, K, Ca, Ti, Cr, Mn, Fe, Cu, Sr, Ba) and nonmetals (F, Si, S, Cl). The observed metallic elements were mostly oligoelements, but toxic elements, such as Al, were

also observed [56]. The authors performed a space-resolved analysis and showed different elemental profiles in different locations in the plants. For example, the highest concentrations of Al, Ca, Ti, Mn, and Fe were found in the skin of the potato, but their concentrations decreased drastically inside the vegetable. The results obtained in this work demonstrated the interest in LIBS analysis for detection and analysis of trace elements in fresh vegetables and more generally in food.

LIBS was employed to determine the spatial distribution of Ag in tissues of treated plants (sunflowers) [57]. The single-shot LIBS analysis was performed along the ~25 mm long *Helianthus annuus* L. stem sections. This study demonstrated the capability of LIBS to trace the uptake of Ag and Cu and to visualize the accumulation trends of different elements in selected structures of the sample, e.g., in the stem, roots or leaves. In this study, Ag was found to accumulate mainly in the near-root part of the sample, unlike Cu, which was more uniformly located in different areas of the stem [57]. Another study evaluated the feasibility of using LIBS to image the presence of Pb, Mg and Cu in leaves of *Helianthus annuus* L. samples [58]. In this work, these common sunflower plants were grown with Pb-doped water solutions a few days before harvesting their leaves. The accumulation of the elements of interest was measured with LIBS and further confirmed with ICP-MS, atomic absorption spectrometry (AAS) and thin layer chromatography (TLC). The authors concluded that the competition between Mg and Pb ions inhibits the magnesium chelatase activity, which thus cannot incorporate Mg ions into newly synthesized chlorophyll molecules. Using a similar strategy, another investigation using LIBS analysis on sunflowers demonstrated that elevated levels of Pb influenced the concentration and distribution of K and Mn within the plant [59]. The authors concluded that Pb competed with K and Mn for binding and absorption sites in the plants.

The use of a femtosecond-LIBS system enabled the element-specific *in situ* investigation of biological samples with high spatial resolution [60]. The authors performed *in situ* measurements of wall-associated calcium ion (Ca^{2+}) distributions within the peripheral cell wall of the sunflower seedling (*Helianthus annuus* L.) stem. In this study, an axial resolution of approximately 100 nm was achieved. The use of femtosecond laser pulses with LIBS also helped to analyze the normal abundance of trace elements, such as Fe, in different compartments of dried maize leaves or fresh leaves of *Cornus stolonifera*, therefore reaching analytical concentration sensitivities as low as 5 ppm [61].

More recently, a LIBS system was developed for in-field deployment. This system directly measured the distribution of multiple elements in living plants and in the soil. The proof-of-concept was achieved through the effective mapping of trace elements from a pesticide that was directly sprayed on maize leaves [62].

The monitoring of plant nutrients (Ca, Fe, Na, K and Mo) in fresh leaves of *Citrus unshiu* and *Rhododendron obtusum* was performed with low-energy LIBS [63]. The metal elements were successfully analyzed with LIBS. However, applying metallic colloidal particles to the surface of the leaves improved the sensitivities and detection limits. In fact, the metallic particles increased the emission intensities via localized surface plasmon phenomenon (Table 1).

Recently, LIBS detected the presence of pesticide residues on the surfaces of agricultural products (fruits) [64]. In addition, it rapidly quantified Ca in different areas of a grain of corn, i.e., the endosperm and embryo of the seed, without any pretreatment procedure. Detection limits of ~1 ppm were achieved for the Ca concentration, which was consistent with atomic absorption fluorescence measurements [65].

Numerous metals have already been analyzed by LIBS in plant materials such as leaves, roots, vegetables or grains. These elements can be either major, minor or even trace elements, and they have been studied in qualitative or semi-quantitative studies. For

an extensive review of all LIBS experiments and the associated elements analyzed in plants, see [66,67].

In summary, space-resolved LIBS is a valuable technique for studying the uptake, transport and, more generally, the role of metal elements in plants. LIBS helps to visualize metal accumulation in specific areas of the plants (space-resolved analysis), which may be of interest in the context of understanding the interactions between plants and their environment. Trace element detection in vegetables also represents an important issue for the assessment and control of food quality and safety [68].

4.2. Preclinical applications

In 2012, our research group proposed a specific methodology for the elemental imaging of metal-based nanoparticles in frozen murine biological tissues [69,70]. One of the most promising applications of LIBS for preclinical studies may be the study of metal-based drugs or NPs (Fig. 4). Therefore, the distribution of the metal-based nanocompounds of interest can be imaged in 2-D at the scale of an entire organ. Importantly, LIBS can directly detect metal NPs, without requiring any chemical modification or labeling with dyes. The screening of elimination organs (i.e., kidney or liver) at different times after administration of metal NPs is a valuable way to perform kinetics studies in animals.

In 2014, the spatial resolution of ~35 μm enabled Gd-based NPs to be assigned to the anatomic structures of murine kidney embedded in epoxy resin [52]. Several elements were imaged (e.g., Fe, Na, Gd, Si, P, Mg, Cu, and Ca, see Table 1) and Gd was predominantly localized in the renal cortex at early time points before being progressively accumulated in the medulla. The effective renal clearance of Gd-NPs was observed one week after the injection (Fig. 4e). These kinetic studies provide information about accumulation, residence time, specific localization within the organ [71] and possibly *in vivo* chemical degradation/stability of the metal-based NPs [52,70]. When endogenous metals are trapped by NPs, changes in their biodistribution may also be demonstrated [72].

In addition to studies evaluating the behavior and elimination of metal-based NPs, LIBS may be of interest for imaging NPs to determine whether they can target tumors. The distribution and tumor penetration of Gd/Si-based [73] and Au-based NPs [74] were recently investigated in paraffin-embedded specimens. The metals of interest (i.e., Gd, Si and Au) and biologically relevant endogenous elements such as P, Fe, Na, Ca, and Mg were imaged (Fig. 4). The penetration depth was measured in a tumor sampled 15 min after the administration of Gd/Si NPs. At this time point, NPs displayed a favorable tumor-to-muscle ratio. LIBS analysis clearly indicated the presence of metal NPs both in the center and at the periphery of tumors, which confirmed previous results obtained with magnetic resonance imaging (MRI).

The lateral resolution achieved is strongly impacted by the nature of the sample. LIBS provided a resolution of 40–100 μm for frozen sections [70,75], whereas a resolution of ~10 μm was achieved for hard epoxy-embedded samples (Fig. 4a) [71]. Although these scanning experiments with LIBS typically result in 2-D projections of the elemental distributions within the sample, they do not provide depth information. To overcome this limitation, we developed a 3-D extension of the 2-D LIBS method. As a proof-of-concept study, we studied the renal kinetics of metal NPs to investigate two different strategies to collect the distribution of elements in 3-D [54]. LIBS was used at the organ scale to image Gd, Ca and Na in a series of adjacent coronal kidney sections. The consecutive images were pooled to reconstruct the organ in 3-D (Fig. 4b). The second approach exploited the ability of LIBS to perform depth profiling via successive shot-to-shot surface ablation. A smaller region of interest was mapped several times with high resolution (10 μm) to obtain the complete 3-D profile. The 3-D profile of metals

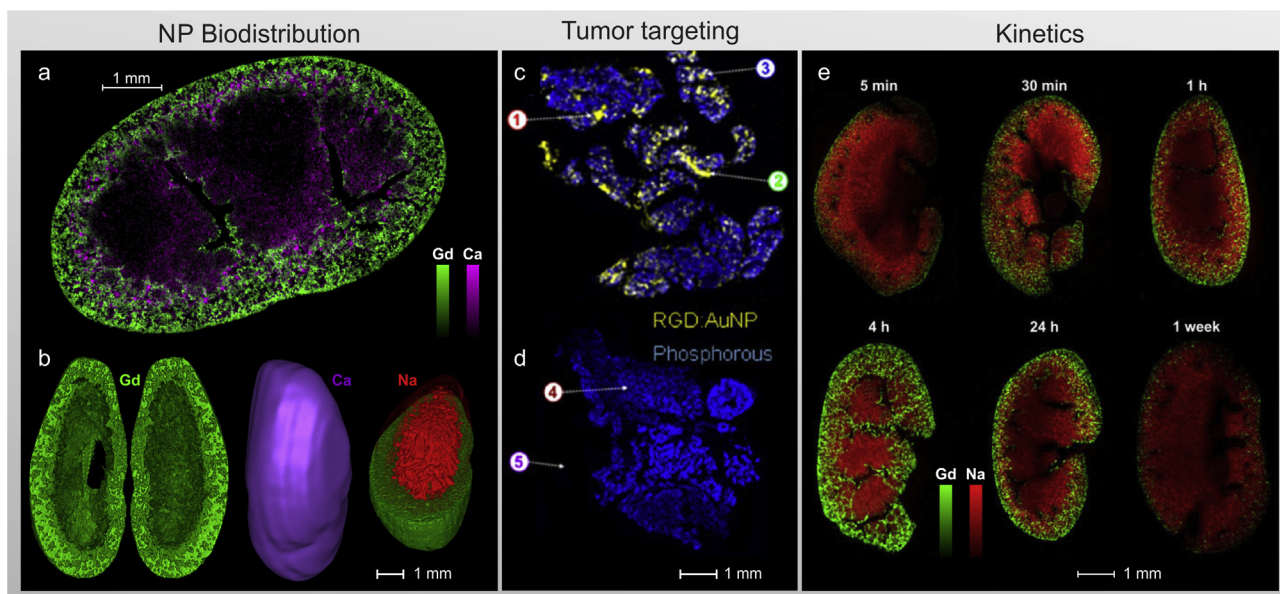


Fig. 4. Localization and quantification of metal-based NPs in kidneys and in tumors. (a) 2-D high resolution elemental map of merged Gd (green) and Ca (purple) in a murine kidney. Adapted with permission from [71]. (b) 3-D distribution of Gd (green) Ca (purple) and Na (red) in a murine kidney. Adapted with permission from [54]. (c and d) Visualization of the effective targeting of Au-NPs in tumors. Au (yellow) and P (blue) elemental images are shown for the Au-NP-treated (c) or untreated (d) tumors. Reprinted with permission from [74] Copyright 2015 American Chemistry Society. (e) Elemental images of Gd (green) and Na (red) in murine kidneys at different time points after the Gd-based NPs administration. Adapted with permission from [52].

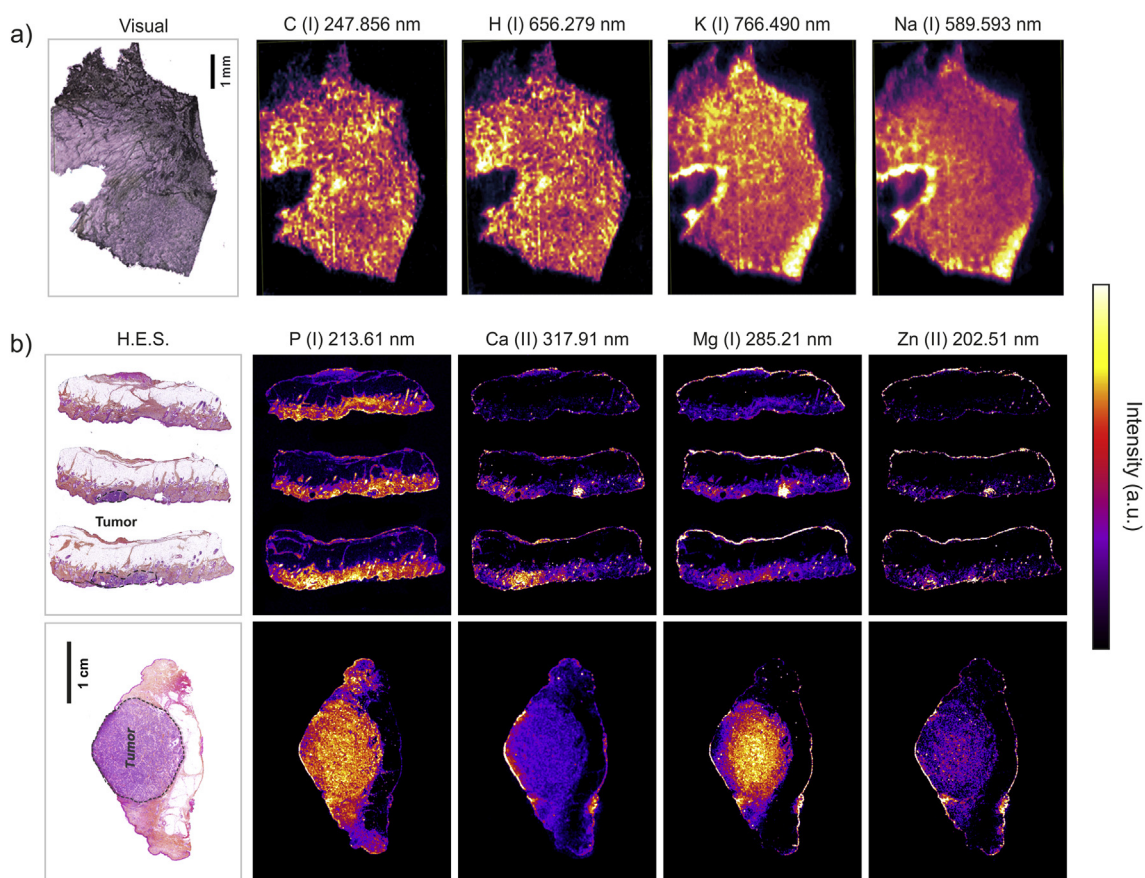


Fig. 5. Tumor analysis via LIBS. (a) Elemental images of C, H, K and Na in a human malignant pleural mesothelioma sample. Modified from [75] with permission. (b) Elemental images for P, Ca, Mg and Zn for a squamous cell carcinoma of the skin (upper row) and Merkel's cell carcinoma (lower row). Modified from [76] with permission.

provided valuable information about the distribution of metal NPs, either at the organ level or within a small restricted area.

4.3. Medical applications

The simultaneous imaging of metal elements in tissues with medical interest has very diverse applications, ranging from the visualization of heterogeneous patterns of endogenous elements to the *in situ* detection of exogenous heavy metals in tissues following occupational or environmental exposure.

Recently, we reported the use of LIBS to record multi-elemental images of human paraffin-embedded skin samples on the entire biopsy scale in a complementary and compatible way with microscope histopathological examination [76]. As described in Table 1, a specific instrumental configuration was proposed to detect most of the endogenous elements of interest (*i.e.*, P, Al, Mg, Na, Zn, Si, Fe, and Cu). In this work, we selected and analyzed different skin biopsies, including healthy skin tissue, cutaneous metastasis of melanoma, Merkel-cell carcinoma and squamous cell carcinoma (Fig. 5b). The elemental images recorded from skin tissues enabled the visualization and identification of the three different physiological layers of the skin, matching perfectly with the expected architecture and organization of the tissue via direct comparison with microscope pathological examination after HES staining.

In the case of metastatic melanoma, the elemental images of the tumor revealed a gradient of concentrations for Ca, P, and Mg, which contrasted with the apparent homogeneous pattern of the tumor cells after histological analysis. The wide dynamic ranges of concentrations for elements, such as Ca, Na, Mg and Fe, with distinct areas presenting low to high concentrations demonstrated the high complementarity of LIBS elemental imaging with conventional histopathology. Importantly, this study was performed on formalin-fixed, paraffin-embedded (FFPE) tissues, which is one of the most frequently archived forms of human material in pathology laboratories, thereby opening new avenues and applications for LIBS metal imaging of samples with medical interest. The simplicity of both the system and procedures justifies the current active development of medical LIBS analysis for diagnostic purposes, especially for metal-related diseases.

We further used LIBS imaging to characterize the presence of exogenous metals in human biopsies embedded in paraffin [77]. In this study, we selected relevant medical situations for which the associated pathology reports were limited to the presence of lymphohistiocytic and inflammatory cells containing granules (one granuloma and one pseudolymphoma) or to lymph nodes or skin tissues containing pigments or foreign substances. Several foreign metal elements such as Al, Ti, Cu, Cr and W were identified and localized within the tissues (Table 1). This work demonstrated that when combined with routine histopathological analysis, LIBS is a versatile technology that might help pathologists establish and/or confirm diagnoses for a wide range of medical applications, particularly when the nature of external agents present in tissues needs to be investigated.

A combination of different techniques may be necessary to obtain complementary information. With this aim, simultaneous LIBS and LA-ICP-MS measurements and image construction have been used for the elemental mapping of trace and bulk elements in frozen human malignant pleural mesothelioma samples [75]. After thoroughly optimizing the method, this tandem LA-ICP-MS/LIBS combination provided elemental distribution images that were interpretable and in good correlation with the histological features of the tumor tissue, thereby demonstrating the applicability of this technique. LIBS was found to be optimal for mapping major elements that are not accessible *via* ICP-MS (*e.g.*, C, O, H) and minor elements that are affected by high background signals

or polyatomic interferences when measured via ICP-MS (*e.g.*, Na, K, Mg, Ca) in biological tissues (Fig. 5a) [75].

Although described with non-biological samples, the first simultaneous 3-D elemental imaging combining LIBS and LA-ICP-MS enabled the spatially resolved mapping of major and trace elements and isotopes in a geological sample [78]. These results suggested that 3-D elemental imaging through simultaneously acquired LIBS and LA-ICP-MS measurements was possible [78]; this finding may bring new applications for 3-D metal analysis of biomedical samples.

The differences between elemental imaging modalities do not mean that all studies should be performed in isolation; on the contrary, the greatest wealth of knowledge may be obtained synergistically via multiple imaging strategies. All these recent breakthroughs provide new perspectives for imaging elements at the entire-organ scale. LIBS and complementary techniques will be required for accurate pre-clinical investigations in the field of metal-based NPs and nanomedicine in general. Regulatory agencies may be interested in the fast, accurate results obtained using LIBS, especially for pre-clinical pharmacokinetic and toxicity studies with metal-based nanoproducts.

5. Conclusions and perspectives

LIBS is an elemental analysis method with potentially wide-ranging applications. Its unique capabilities enable analyzing major/minor/trace metal elements in various biological materials. The information collected is analyzed to qualitatively and quantitatively measure materials by monitoring their positions and intensities, thus enabling the observation of enriched or depleted metal distributions according to the location in the organism or to its exposure. Elemental analysis via LIBS is simple and fast. LIBS is complementary to other existing methods for multi-elemental imaging, each one achieving different resolution or sensitivity. Although minimally destructive to the sample [3], LIBS analysis is accessible in standard laboratory settings for any type of sample. To conduct reproducible LIBS imaging analysis, it is first critical to avoid any surface contamination when preparing the sample. In addition, instrumental parameters (such as laser energy and positioning of the sample surface with regard to the laser focus), must be controlled and kept constant during the entire experiment. LIBS imaging requires high levels of instrumentation controls, including at least systems for stabilizing both the laser energy and the laser focusing. It is also important to mention that the quantitative calibration is not always possible depending on the availability of standards. However, researches are currently conducted in different laboratories to make LIBS technology more reliable in the quantitative point of view.

In addition, LIBS imaging can be combined with other imaging modalities such as Raman spectroscopy [79,80] or laser-induced fluorescence [81,82]. These multi-modal approaches are very promising since they can collect complementary information about the nature of the samples. A combination of LA-ICP-MS and LIBS was used for laterally resolved elemental analysis of biological samples [75]. LA-ICP-MS and LIBS are both based on laser ablation. LA-ICP-MS enables the identification of isotopes in certain conditions and may be more sensitive. LIBS is all-optical and has no restriction on the analysis of low atomic number elements. LIBS can also screen clinical paraffin-embedded specimens within a few minutes [76,77].

Importantly, the global understanding of metal element distributions requires a direct comparison between optical microscopy images of the tissue with elemental images. This helps properly visualize the area of interest with anatomical and pathological information. Images obtained from histology and different

elemental imaging technologies can be merged [76,77,83]. This important step will undeniably contribute to the widespread use of LIBS for investigating the presence or role of metals in biological and medical samples.

LIBS elemental imaging may be entering a new era in which laboratories interested in the role of metals will increasingly use it as a versatile tool to image, monitor, and understand unexpected patterns or heterogeneous spatial distributions in 2-D or in 3-D. The future availability of commercial LIBS systems will undeniably broaden its use for research or medical purposes, and the innumerable applications of LIBS imaging will eventually outshine the selected biological, pre-clinical and medical aspects described in this review.

Conflicts of interests

None.

Funding

This work was supported by the ITMO Cancer et ITMO Technologies pour la santé de l'alliance nationale pour les sciences de la vie et de la santé (AVIESAN), the Institut National du Cancer (INCa) and INSERM within the project LAST (#PC201513). This work was also supported by the grant ANR-17-CE18-0028 "MEDI-LIBS".

References

- [1] D.A. Rusak, B.C. Castle, B.W. Smith, J.D. Winefordner, *Crit. Rev. Anal. Chem.* 27 (1997) 257–290.
- [2] S.C. Jantzi, V. Motto-Ros, F. Trichard, Y. Markushin, N. Melikechi, A. De Giacomo, *Spectrochim. Acta, Part B* 115 (2016) 52–63.
- [3] D.W. Hahn, N. Omenetto, *Appl. Spectrosc.* 66 (2012) 347–419.
- [4] D.A. Cremers, R.C. Chinni, *Appl. Spectrosc. Rev.* 44 (2009) 457–506.
- [5] A.P.M. Michel, *Spectrochim. Acta, Part B* 65 (2010) 185–191.
- [6] Y. Deguchi, Z. Wang, *Industrial applications of laser-induced breakdown spectroscopy*, in: T. Mieno (Ed.), *Plasma Science and Technology – Progress in Physical States and Chemical Reactions*, InTech, Rijeka, 2016, Ch. 15.
- [7] N.J. McMillan, S. Rees, K. Kochelek, C. McManus, *Geostand. Geoanal. Res.* 38 (2014) 329–343.
- [8] S. Qiao, Y. Ding, D. Tian, L. Yao, G. Yang, *Appl. Spectrosc. Rev.* 50 (2015) 1–26.
- [9] V.K. Singh, V. Singh, A.K. Rai, S.N. Thakur, P.K. Rai, J.P. Singh, *Appl. Opt.* 47 (2008) G38–G47.
- [10] B.G. Oztoprak, J. Gonzalez, J. Yoo, T. Gulecen, N. Mutlu, R.E. Russo, O. Gundogdu, A. Demir, *Appl. Spectrosc.* 66 (2012) 1353–1361.
- [11] V.K. Singh, V. Kumar, J. Sharma, *Lasers Med. Sci.* 30 (2015) 1763–1778.
- [12] V.K. Singh, A.K. Rai, *Lasers Med. Sci.* 26 (2011) 673–687.
- [13] A. Kumar, F.-Y. Yueh, J.P. Singh, S. Burgess, *Appl. Opt.* 43 (2004) 5399–5403.
- [14] F. Ghasemi, P. Parvin, N.S. Hosseini Motlagh, A. Amjadi, S. Abachi, *Appl. Opt.* 55 (2016) 8227–8235.
- [15] A. El-Husseini, A.K. Kassem, H. Ismail, M.A. Harith, *Talanta* 82 (2010) 495–501.
- [16] J.H. Han, Y. Moon, J.J. Lee, S. Choi, Y.C. Kim, S. Jeong, *Biomed. Opt. Express* 7 (2016) 57–66.
- [17] Y. Markushin, P. Sivakumar, D. Connolly, N. Melikechi, *Anal. Bioanal. Chem.* 407 (2015) 1849–1855.
- [18] J. Peng, K. Song, H. Zhu, W. Kong, F. Liu, T. Shen, Y. He, *Sci. Rep.* 7 (2017) 44551.
- [19] R. Kanawade, F. Mehari, C. Knipfer, M. Rohde, K. Tangermann-Gerk, M. Schmidt, F. Stelzle, *Spectrochim. Acta, Part B* 87 (2013) 175–181.
- [20] F. Mehari, M. Rohde, R. Kanawade, C. Knipfer, W. Adler, F. Klämpfl, F. Stelzle, M. Schmidt, *J. Biophotonics* 9 (2016) 1021–1032.
- [21] Z. Grolmusová, M. Hornáčková, J. Plavčan, M. Kopáni, P. Babál, P. Veis, *Eur. Phys. J. Appl. Phys.* 63 (2013).
- [22] C.J. Chang, *Nat. Chem. Biol.* 11 (2015) 744–747.
- [23] K.J. Waldron, J.C. Rutherford, D. Ford, N.J. Robinson, *Nature* 460 (2009) 823–830.
- [24] J.F. Collingwood, F. Adams, *Spectrochim. Acta, Part B: At. Spectrosc.* (2017).
- [25] W. Maret, *Int. J. Mol. Sci.* 17 (2016).
- [26] C.M. Ackerman, S. Lee, C.J. Chang, *Anal. Chem.* 89 (2017) 22–41.
- [27] R. McRae, P. Bagchi, S. Sumalekshmy, C.J. Fahrni, *Chem. Rev.* 109 (2009) 4780–4827.
- [28] K.M. Dean, Y. Qin, A.E. Palmer, *BBA* 1823 (2012) 1406–1415.
- [29] Y. Choi, Y. Park, T. Kang, L.P. Lee, *Nat. Nanotechnol.* 4 (2009) 742–746.
- [30] L. Hao, J. Li, A. Kappler, M. Obst, *Appl. Environ. Microbiol.* 79 (2013) 6524–6534.
- [31] D.L. Ma, H.Z. He, H.J. Zhong, S. Lin, D.S. Chan, L. Wang, S.M. Lee, C.H. Leung, C.Y. Wong, *ACS Appl. Mater. Interfaces* 6 (2014) 14008–14015.
- [32] S. Lin, C. Yang, Z. Mao, B. He, Y.T. Wang, C.H. Leung, D.L. Ma, *Biosens. Bioelectron.* 77 (2016) 609–612.
- [33] W. Wang, Z. Mao, M. Wang, L.J. Liu, D.W. Kwong, C.H. Leung, D.L. Ma, *Chem. Commun. (Camb.)* 52 (2016) 3611–3614.
- [34] P. Miao, Y. Tang, L. Wang, *ACS Appl. Mater. Interfaces* 9 (2017) 3940–3947.
- [35] D.J. Hare, E.J. New, M.D. de Jonge, G. McColl, *Chem. Soc. Rev.* 44 (2015) 5941–5958.
- [36] K.J. Barnham, A.I. Bush, *Chem. Soc. Rev.* 43 (2014) 6727–6749.
- [37] A. Sussulini, J.S. Becker, J.S. Becker, *Mass Spectrom. Rev.* 36 (2017) 47–57.
- [38] M. Dehnhardt, M.V. Zoriy, Z. Khan, G. Reifengerber, T.J. Ekström, J. Sabine Becker, K. Zilles, A. Bauer, *J. Trace Elem. Med. Biol.* 22 (2008) 17–23.
- [39] J. Dobrowolska, M. Dehnhardt, A. Matusch, M. Zoriy, N. Palomero-Gallagher, P. Koscielniak, K. Zilles, J.S. Becker, *Talanta* 74 (2008) 717–723.
- [40] M.V. Zoriy, M. Dehnhardt, A. Matusch, J.S. Becker, *Spectrochim. Acta, Part B* 63 (2008) 375–382.
- [41] M.M. Niedzwiecki, C. Austin, R. Remark, M. Merad, S. Gnjatic, G. Estrada-Gutierrez, A. Espejel-Nunez, H. Borboa-Olivares, M. Guzman-Huerta, R.J. Wright, R.O. Wright, M. Arora, *Metallomics* 8 (2016) 444–452.
- [42] R. Gonzalez de Vega, M.L. Fernandez-Sanchez, J. Pisonero, N. Eiro, F.J. Vizoso, A. Sanz-Medel, *J. Anal. At. Spectrom.* 32 (2017) 671–677.
- [43] J. Anyz, L. Vyslouzilova, T. Vaculovic, M. Tvrdonova, V. Kanicky, H. Haase, V. Horak, O. Stepankova, Z. Heger, V. Adam, *Sci. Rep.* 7 (2017) 40169.
- [44] M.W. Bourassa, L.M. Miller, *Metallomics* 4 (2012) 721–738.
- [45] L. Perrin, S. Roudeau, A. Carmona, F. Domart, J.D. Petersen, S. Bohic, Y. Yang, P. Cloetens, R. Ortega, *ACS Chem. Neurosci.* 8 (2017) 1490–1499.
- [46] K.M. Davies, D.J. Hare, S. Bohic, S.A. James, J.L. Billings, D.I. Finkelstein, P.A. Doble, K.L. Double, *Anal. Chem.* 87 (2015) 6639–6645.
- [47] S.A. James, D.J. Hare, N.L. Jenkins, M.D. de Jonge, A.I. Bush, G. McColl, *Sci. Rep.* 6 (2016) 20350.
- [48] J.F. Collingwood, R.K.K. Chong, T. Kasama, R.E. Dunin-Borkowski, G. Perry, M. Posfai, S. Siedlak, E.T. Simpson, M.A. Smith, J. Dobson, *J. Alzheimers Dis.* 14 (2008) 235–245.
- [49] S. Yumoto, S. Kakimi, A. Ohsaki, A. Ishikawa, *J. Inorg. Biochem.* 103 (2009) 1579–1584.
- [50] F.J. Fortes, J. Moros, P. Lucena, L.M. Cabalin, J.J. Laserna, *Anal. Chem.* 85 (2013) 640–669.
- [51] G. Galbács, *Anal. Bioanal. Chem.* 407 (2015) 7537–7562.
- [52] L. Sancey, V. Motto-Ros, B. Busser, S. Kotb, J.M. Benoit, A. Piednoir, F. Lux, O. Tillement, G. Panczer, *J. Yu, Sci. Rep.* 4 (2014) 6065.
- [53] H. Bette, R. Noll, *J. Phys. D Appl. Phys.* 37 (2004) 1281.
- [54] Y. Gimenez, B. Busser, F. Trichard, A. Kulesza, J.M. Laurent, V. Zaun, F. Lux, J.M. Benoit, G. Panczer, P. Dugourd, O. Tillement, F. Pelascini, L. Sancey, V. Motto-Ros, *Sci. Rep.* 6 (2016) 29936.
- [55] D.K. Chauhan, D.K. Tripathi, N.K. Rai, A.K. Rai, *Food Biophys.* 6 (2011) 416–423.
- [56] V. Juvé, R. Portelli, M. Boueri, M. Baudelet, J. Yu, *Spectrochim. Acta, Part B* 63 (2008) 1047–1053.
- [57] S. Krizkova, P. Ryant, O. Krystofova, V. Adam, M. Galiova, M. Beklova, P. Babula, J. Kaiser, K. Novotny, J. Novotny, M. Liska, R. Malina, J. Zehnalek, J. Hubalek, L. Havel, R. Kizek, *Sensors (Basel)* 8 (2008) 445–463.
- [58] J. Kaiser, M. Galiova, K. Novotny, R. Cervenka, L. Reale, J. Novotny, M. Liska, O. Samek, V. Kanicky, A. Hrdlicka, K. Stejskal, V. Adam, R. Kizek, *Spectrochim. Acta, Part B: At. Spectrosc.* 64 (2009) 67–73.
- [59] M. Galiová, J. Kaiser, K. Novotný, O. Samek, L. Reale, R. Malina, K. Páleníková, M. Liška, V. Čudek, V. Kanický, V. Otruba, A. Poma, A. Tucci, *Spectrochim. Acta, Part B* 62 (2007) 1597–1605.
- [60] A. Assion, M. Wollenhaupt, L. Haag, F. Mayorov, C. Sarpe-Tudoran, M. Winter, U. Kutschera, T. Baumert, *Appl. Phys. B* 77 (2003) 391–397.
- [61] O. Samek, J. Lambert, R. Hergenroder, M. Liška, J. Kaiser, K. Novotný, S. Kulkhreshy, *Laser Phys. Lett.* 3 (2006) 21.
- [62] C. Zhao, D. Dong, X. Du, W. Zheng, *Sensors (Basel)* 16 (2016).
- [63] T. Ohta, M. Ito, T. Kotani, T. Hattori, *Appl. Spectrosc.* 63 (2009) 555–558.
- [64] X. Du, D. Dong, X. Zhao, L. Jiao, P. Han, Y. Lang, *RSC Adv.* 5 (2015) 79956–79963.
- [65] P. Han, D. Dong, X. Du, L. Jiao, X. Zhao, *Anal. Methods* 8 (2016) 6705–6710.
- [66] D. Santos, L.C. Nunes, G.G.A. de Carvalho, M.D.S. Gomes, P.F. de Souza, F.D.O. Leme, L.G.C. dos Santos, F.J. Krug, *Spectrochim. Acta, Part B: At. Spectrosc.* 71 (2012) 3–13.
- [67] J. Kaiser, K. Novotný, M.Z. Martin, A. Hrdlička, R. Malina, M. Hartl, V. Adam, R. Kizek, *Surf. Sci. Rep.* 67 (2012) 233–243.
- [68] M. Markiewicz-Keszycza, X. Cama-Moncuñil, M.P. Casado-Gavaldá, Y. Dixit, R. Cama-Moncuñil, P.J. Cullen, C. Sullivan, *Trends Food Sci. Technol.* 65 (2017) 80–93.
- [69] V. Motto-Ros, L. Sancey, Q.L. Ma, F. Lux, X.S. Bai, X.C. Wang, J. Yu, G. Panczer, O. Tillement, *Appl. Phys. Lett.* 101 (2012) 223702.
- [70] V. Motto-Ros, L. Sancey, X.C. Wang, Q.L. Ma, F. Lux, X.S. Bai, G. Panczer, O. Tillement, J. Yu, *Spectrochim. Acta, Part B* 87 (2013) 168–174.
- [71] L. Sancey, S. Kotb, C. Truillet, F. Appaix, A. Marais, E. Thomas, B. van der Sanden, J.-P. Klein, B. Laurent, M. Cottier, R. Antoine, P. Dugourd, G. Panczer, F. Lux, P. Perriat, V. Motto-Ros, O. Tillement, *ACS Nano* 9 (2015) 2477–2488.
- [72] A. Moussaron, S. Vibhute, A. Bianchi, S. Gündüz, S. Kotb, L. Sancey, V. Motto-Ros, S. Rizzitelli, Y. Crémillieux, F. Lux, N.K. Logothetis, O. Tillement, G. Angelovski, *Small* 11 (2015) 4900–4909.
- [73] A. Detappe, S. Kunjachan, L. Sancey, V. Motto-Ros, D. Biancur, P. Drane, R. Guieze, G.M. Makrigrigios, O. Tillement, R. Langer, R. Berbeco, *J. Control. Release* 238 (2016) 103–113.

- [74] S. Kunjachan, A. Detappe, R. Kumar, T. Ireland, L. Cameron, D.E. Biancur, V. Motto-Ros, L. Sancey, S. Sridhar, G.M. Makrigiorgos, R.I. Berbeco, *Nano Lett.* 15 (2015) 7488–7496.
- [75] M. Bonta, J.J. Gonzalez, C.D. Quarles, R.E. Russo, B. Hegedus, A. Limbeck, *J. Anal. At. Spectrom.* 31 (2016) 252–258.
- [76] S. Moncayo, F. Trichard, B. Busser, M. Sabatier-Vincent, F. Pelascini, N. Pinel, I. Templier, J. Charles, L. Sancey, V. Motto-Ros, *Spectrochim. Acta, Part B* 133 (2017) 40–44.
- [77] B. Busser, S. Moncayo, F. Trichard, V. Bonnetterre, N. Pinel, F. Pelascini, P. Dugourd, J. Coll, M. D'Incan, J. Charles, V. Motto-Ros, L. Sancey, *Mod. Pathol.* (2017), <https://doi.org/10.1038/modpathol.2017.1152>, in press.
- [78] J.R. Chirinos, D.D. Oropeza, J.J. Gonzalez, H. Hou, M. Morey, V. Zorba, R.E. Russo, *J. Anal. At. Spectrom.* 29 (2014) 1292–1298.
- [79] K.M.M. Shameem, K.S. Choudhari, A. Bankapur, S.D. Kulkarni, V.K. Unnikrishnan, S.D. George, V.B. Kartha, C. Santhosh, *Anal. Bioanal. Chem.* 409 (2017) 3299–3308.
- [80] J. Moros, J.A. Lorenzo, P. Lucena, L. Miguel Tobarria, J.J. Laserna, *Anal. Chem.* 82 (2010) 1389–1400.
- [81] J. Li, Z. Hao, N. Zhao, R. Zhou, R. Yi, S. Tang, L. Guo, X. Li, X. Zeng, Y. Lu, *Opt. Express* 25 (2017) 4945–4951.
- [82] X.K. Shen, H. Wang, Z.Q. Xie, Y. Gao, H. Ling, Y.F. Lu, *Appl. Opt.* 48 (2009) 2551–2558.
- [83] R. Van de Plas, J. Yang, J. Spraggins, R.M. Caprioli, *Nat. Methods* 12 (2015) 366–372.